Characterization of Organic Coatings on Metal Substrates by Electrochemical Impedance Spectroscopy ☆

J. Titz, G.H. Wagner,* H. Spähn,* M. Ebert,** K. Jüttner,** and W.J. Lorenz***

ABSTRACT

Organic coatings on phosphated and bare mild steel exposed to aqueous sodium chloride solutions were investigated by electrochemical impedance spectroscopy (EIS). The corrosion protection of coatings is well characterized by a thorough transfer function analysis of the EIS data obtained. A quasi-homogeneous and two different inhomogeneous three-dimensional surface models were used to analyze perfect and imperfect coatings, respectively. Local defects within the organic coatings and delamination effects at the substrate/coating interface were determined quantitatively even after a relatively short exposure time.

KEY WORDS: impedance spectroscopy, organic coatings, transfer function analysis.

INTRODUCTION

Painting or coating with organic matters is a widespread method to provide corrosion protection and to improve the durability of engineering structures. Localized corrosion processes caused by inhomogeneities within the three-dimensional (3-D) film are the most frequent reasons for damages on metal surfaces protected by thin organic coatings. Such inhomogeneities can be mechanical damages, pores, or merely a weakening of the coating, e.g., electrolytically conductive pathways. Furthermore, from a practical point of view, the strength of the bonding of such coatings—especially after damage—to the metal substrate is of outstanding importance for the protection quality.

Atmospheric accelerated testing methods such as salt spray and climate changing tests are usually applied to characterize organic coatings on metal substrates in the laboratory. These procedures are rather time consuming until reliable results are obtained, which nevertheless often lack correlations with practical experience. Despite the extensive use of organic coatings, no other generally accepted short-time tests exist for practical applications to assess the corrosion protective performance of organic coatings and paints. This lack hinders research and development work for formulating new and improved commercial coating and paint products.

Since metallic corrosion in aqueous solutions is mostly an electrochemical phenomenon, electrochemical test methods are useful to assess the ability of a coating or paint to prevent corrosion. Consequently, electrochemical measurements of polarization phenomena of the system metal/coating or film/electrolyte have been applied for a long time. However, standard electrochemical direct current (DC) techniques have appeared to be poorly reproducible and, in the case of nearly perfect coatings, even impracticable. Furthermore, these methods are likely to introduce measurement errors due to potential drops across the high-resistance organic film. Large-signal perturbation techniques of the conventional electrochemical test methods may cause polarization effects at the electrode/coating interface leading to irreversible changes of the system concerned. However, electrochemical impedance spectroscopy (EIS) as a small signal perturbation technique has proved to be a powerful tool to obtain system-specific parameters of coatings and paints.[1–4] EIS represents an *in situ* technique that allows one to detect surface inhomogeneities correlated to the corrosion process as a function of the exposure time. The interpretation of experimental EIS data by means of a transfer function analysis based on an appropriate physical model of the corrosion process at the metal/coating interface may lead to a better understanding of local corrosion mechanisms. A computer fit of the theoretical transfer function to the experimental EIS data can yield system-specific parameters that allow a comprehensive interpretation of the corrosion performance of organic coatings and films.

Different models have been described to interpret EIS data of coated metals.[5–14] However, these models have to be considered as qualitative approximations. In addition, there are only a few investigations on high-performance commercial grade coatings and paints.[15] Such real systems generally show a more complicated behavior than the model systems often used in laboratory tests.

In this work EIS is applied as an appropriate short-time test procedure to assess and predict the corrosion protection behavior of industrial organic coatings electrodeposited on bare and phosphated steel. The results are interpreted by a transfer-function analysis based on an inhomogeneous 3-D surface model in order to obtain parameters characterizing quantitatively the coating performance.

☆ Submitted for publication April 1989; in revised form, August 1989.

* BASF AG, D-6700 Ludwigshafen, FRG.

**Institute of Physical Chemistry and Electrochemistry, University of Karlsruhe, Kaiserstrasse 12, D-7500 Karlsruhe, FRG.

0010-9312/90/000069/$3.00/0

EXPERIMENTAL

Preparation of Electrocoatings

Cured, lead pigmented, epoxy-resin based coatings (BASF[1] product under development) of about 20-μm thickness electrodeposited in a pilot plant facility on bare and phosphated mild steel were studied in aerated 0.5 M NaCl solution (analytical grade, Merck)[2] at room temperature. Coatings obtained from two batches and showing different protection properties in conventional corrosion tests were used in the present study and are denoted as (A) and (B) in the following.

Prior to each experiment, the coated specimens were degreased with acetone and rinsed with deionized water. The short-time contact of acetone with the coating did not affect the coating quality and the experimental results.

Measurements were also performed on coated samples with drilled pores of 0.01-cm diameter in order to study coatings with defined defects.

Experimental Setup

The electrochemical cell is schematically shown in Figure 1. The area of the working electrode exposed to the electrolyte was $\mathbf{A} = 20\ cm^2$. A platinum gauze and a Hg/Hg_2Cl_2 (KCl, saturated) electrode served as counter and reference electrodes, respectively. For EIS measurements, a platinum probe was coupled through a 10 μF capacitor with the reference electrode. The cell was placed into a Faraday cage in order to improve the signal-to-noise ratio.

EIS measurements in the frequency range $10^{-3} \leq f \leq 10^5$ Hz were carried out using a frequency response analyzer (Solartron[3] 1174) and a specially developed potentiostat (BASF). The measurements were digitally controlled by a computer system (DEC[4] PDP 11/73) using a fully automated measuring routine. Transfer function analysis was performed applying nonlinear fit routines.[16]

Measuring Routine

EIS measurements were carried out under potentiostatic control at the open-circuit potential as a function of the exposure time, 15 min $\leq t \leq$ 264 h. The open-circuit potential was measured for $t \approx 15$ min prior to each EIS measurement.

For disbonding experiments, the sample was held at a constant cathodic potential of $E_{SCE} = -1250$ mV. This cathodic polarization was interrupted for EIS measurements, which were started after attaining a steady-state open-circuit potential within about 15 minutes.

A logarithmic repartition of 8 frequency points per decade was chosen with a measuring time of 10 sec or one total oscillation per point for lower frequency values. The amplitude of the sinusoidal system perturbation was $3 \leq \Delta E \leq 10$ mV rms, the current ranges of the potentiostat were set according to the changing impedance values. At lower frequency ranges, appropriate low-pass filters were used to suppress noise.[17,18] Furthermore, to minimize the measuring time, only the current signal was measured at frequencies $f \leq 10$ Hz and correlated to the output signal of the frequency response analyzer (equipped with only one correlator). Because potentiostats do not generate any potential phase shift or amplitude attenuation at low frequencies, it is not necessary to measure the potential signal in the low-frequency range separately. The time stability of the systems studied was checked by reversing the frequency sweep.

For the interpretation of the measurements, the technical limitations of the data collection has to be taken into account. Thus,

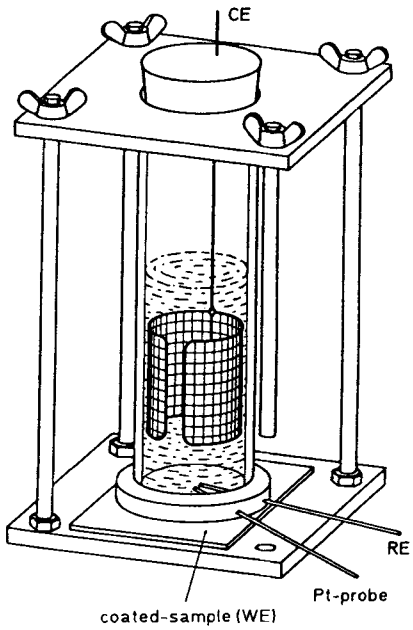

FIGURE 1. *Electrochemical cell. WE = working electrode, CE = counter electrode, RE = reference electrode.*

the low-frequency part of the diagram can only be measured on rather thin and/or imperfect coatings with an absolute DC coating resistance of $R \leq 10^{10}\ \Omega$ using highly sophisticated current amplifiers. At higher coating resistances, the impedance data are limited by the input impedance of about $10^{12}\ \Omega$ of the potential-measuring field-effect transistors within the potentiostat. Additional limitations may result from input protection circuits and atmospheric pollution deposits on the electronic circuits.

Similarly, the complete high-frequency part of the diagrams up to the high-frequency breakpoint, f_h, of the coating capacitance C_L with the ohmic cell resistance R_Ω[5] cannot be measured because of the bandwidth limitation of the measuring device. It can easily be calculated that f_h is about at $f \geq 8$ MHz for a coating thickness of about 20 μm.[17]

RESULTS AND DISCUSSION

Typical impedance spectra of an organic coating (A) deposited on phosphated steel are shown in Figure 2.

Curve (a) corresponds to a quasi-ideal coating and does not undergo any substantial variation even after an extended exposure time up to half a year. A quasi-capacitive behavior with a high-polarization resistance in the order of magnitude of the measuring limit (see previous section, Measuring Routine) is observed corresponding to only one time constant. From the thickness of the organic coating and the measured capacitance, a dielectric constant of $\epsilon \approx 4.8 \pm 0.3$ is evaluated.

Curves (b) and (c) were obtained on a nonperfect coating due to a relatively poor application quality. In this case, the Bode diagrams exhibit significant changes even after relatively short exposure times. With increasing exposure time, the polarization resistance decreases and an additional plateau develops at medium frequencies as seen in the log Z vs log f plots. This plateau corresponds to a minimum in the phase angle ϕ vs log f plots. The break points in the log Z vs log f plots correspond to inflection points in the ϕ vs log f plots indicating the different time constants.

(1) BASF AG, Ludwigshafen, FRG.

(2) Merck and Co., Inc., Rahway, NJ.

(3) Solartron Instrumentation Group, Sangamo Weston Inc., Irvine, CA.

(4) Digital Equipment Corporation (DEC), Maynard, MA.

(5) Under the given experimental conditions, the ohmic resistance was found to be $R_\Omega \approx 20\ \Omega cm^2$ by measuring the solution resistance in the electrochemical cell on a bare steel sheet. Typical organic coating layer capacitances are in the order of magnitude of $C_L \leq 10^{-9}\ Fcm^{-2}$.

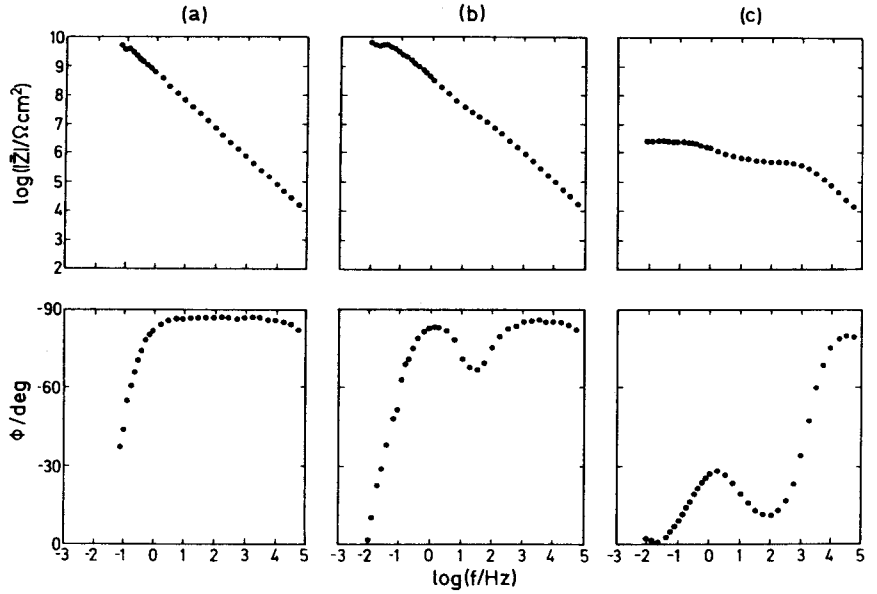

FIGURE 2. *Bode plots of organic coating A on phosphated steel. Quasi-ideal coating (a), non-perfect coatings after exposure times: 1 h (b); 48 h (c).*

A perfect dielectric coating can be described by the quasi-homogeneous 3-D layer Model A (Figure 3). Its transfer function Z_L (corrected for R_Ω) is well approximated by a parallel combination of the organic coating layer capacitance, C_L, and the organic coating layer resistance, R_L:

$$Z_L(s)^{-1} = Y_L(s) = R_L^{-1} + sC_L \quad (1)$$

where $Y_L(s)$ denotes the admittance and $s = j\omega$ with $\omega = 2\pi f$. In the case of a highly resistive coating, Z_L is mainly determined by the capacitance C_L.

A fit of the experimental curve (a) in Figure 2 using Equation (1) with $R_\Omega = 20\ \Omega\cdot cm^2$ is shown in Figure 4. As can be seen, the fit deviates at higher frequencies from the experimental data. This is due to phase errors introduced by the electronic setup under high capacitive load leading to a small frequency dispersion. Therefore, the quality of the fit is improved slightly by use of the dispersion formula:[1,19]

$$Z_L(s) = R_L\,[1 + (sC_LR_L)^\alpha]^{-1} \quad (2)$$

with the empirical exponent α ($0 \leq \alpha \leq 1$) as demonstrated in Figure 5. The values C_L and R_L can be considered as typical parameters for the undamaged coating. R_Ω and R_L are used as invariable parameters in the following fits of nonperfect coatings.

In the presence of local defects, the coating behavior can be described by an inhomogeneous 3-D layer model.[20–22] In this case, the transfer function Z(s) consists of a parallel combination of the impedance of the undamaged film areas $Z_L(s)$ and that of conductive pathways $Z_{corr}(s)$. In a first approximation, the admittances of both values are weighted by the degree of coverage θ in the following way:

$$Z(s)^{-1} = Y(s) = \theta Y_L(s) + (1 - \theta)Y_{corr}(s) \quad (3)$$

where Y(s) and $Y_L(s)$ represent the overall admittance and the layer admittance, whereas $Y_{corr}(s)$ denotes the admittance of the corrosion process that occurs at the substrate/electrolyte interface at the bottom of "virtual pores" within the film. In particular, $Y_{corr}(s)$ is given by

$$Y_{corr}(s)^{-1} = Z_{corr}(s) = R_{\Omega,por} + Z_{SR}(s)[1 + sZ_{SR}(s)C_{dl}]^{-1} \quad (4)$$

where $R_{\Omega,por}$ represents an electrolyte resistance within virtual or real pores, Z_{SR} is the impedance of the surface reactions, and C_{dl} is the electrochemical double-layer capacitance at the bottom of the pores. In principle, corrosion reactions are considered to consist of uncoupled anodic and cathodic partial reactions. Therefore, the impedance $Z_{SR}(s)$ can be described by a parallel combination of $Z_{SR,a}(s)$ and $Z_{SR,c}(s)$ corresponding to the anodic and cathodic partial reactions:

$$Z_{SR}(s)^{-1} = Z_{SR,a}(s)^{-1} + Z_{SR,c}(s)^{-1} \quad (5)$$

The surface reaction impedances $Z_{SR,a}(s)$ and $Z_{SR,c}(s)$ are, in general, complex functions determined by charge transfer, mass transport, chemical reactions, and electrocrystallization steps.

In a first approximation, $Z_{SR}(s)$ can be replaced by the polarization resistance R_p of the corrosion process (Model B, Figure 6):

$$Y_{corr}(s)^{-1} = Z_{corr}(s) \approx R_{\Omega,por} + R_p[1 + sR_pC_{dl}]^{-1} \quad (6)$$

Figure 7 shows a fit of curves (b) and (c) in Figure 2 using Equations (2), (3), and (6), $R_\Omega = 20\ \Omega\cdot cm^2$, and R_L from the fit of the perfect film according to Equation (2). Fit and experimental data deviate more significantly for curve (c) than curve (b).

A much better fit for curve (c) is achieved using the dispersion formula

$$Y_{corr}(s)^{-1} = Z_{corr}(s) \approx R_{\Omega,por} + R_p[1 + (sR_pC_{dl})^{\alpha'}]^{-1} \quad (7)$$

as shown in Figure 8.

Fit parameters determined for the two different coatings (A) and (B) on bare and phosphated mild steel depending on the exposure time are listed in Table 1a. From the $(1 - \theta)C_{dl}$ values in Table 1a, the value of θ can be calculated assuming a constant value of $C_{dl} = 25 \times 10^{-6}\ F\cdot cm^{-2}$, which is reasonable for a bare and quasi-homogeneous iron metal surface in contact with NaCl electrolyte.[23,24] Then, the specific parameters C_L, $R_{\Omega,por}$, R_p, and the active surface area $(1 - \theta)\mathbf{A}$ can also be evaluated. These data are listed in Table 1b.

Principally, in the case of delamination effects, the active area at the metal/coating interface $(1 - \theta_1)\mathbf{A}$ increases with the exposure time, whereas the area at the coating/electrolyte interface $(1 - \theta_2)\mathbf{A}$ corresponding to the number and geometry of coating defects varies much less as can be seen by optical means. Using θ_1 instead of θ_2 causes only insignificant errors in

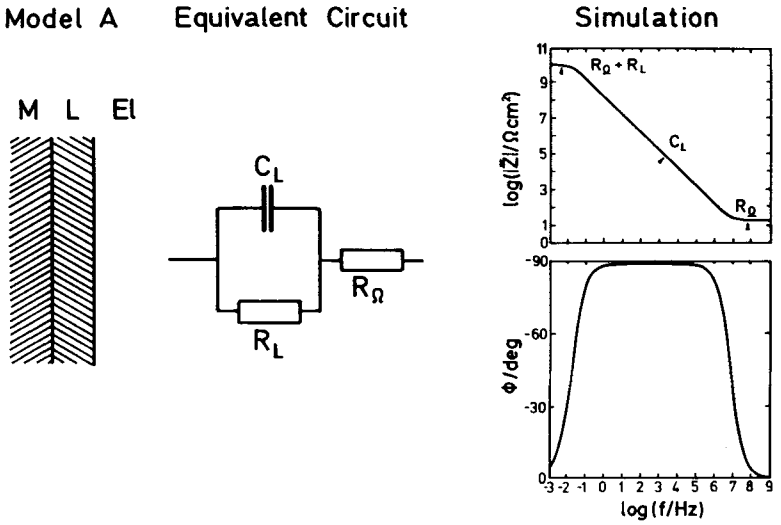

FIGURE 3. *Quasi-homogeneous 3-D surface layer Model A according to Equation (1). M: metal substrate; L: layer of organic coating; El: electrolyte. Simulation parameters: R_Ω = 20 Ω·cm², R_L = 10^{10} Ω·cm², C_L = 10^{-9} F·cm^{-2}.*

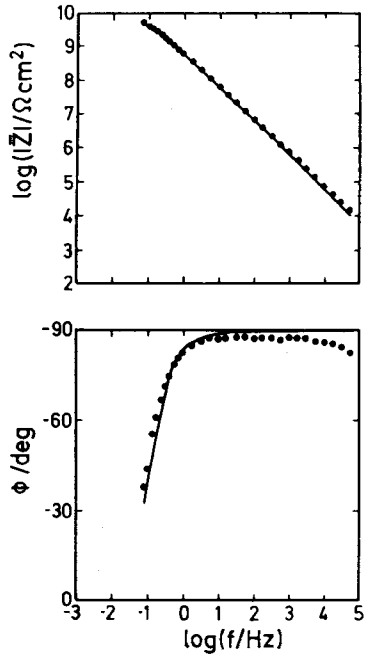

FIGURE 4. *Fit of the experimental data of curve (a) in Figure 2 with Model A according to Equation (1). Fit parameters: R_L = 5.5 × 10^9 Ω·cm², C_L = 2.4 × 10^{-10} F·cm^{-2}.*

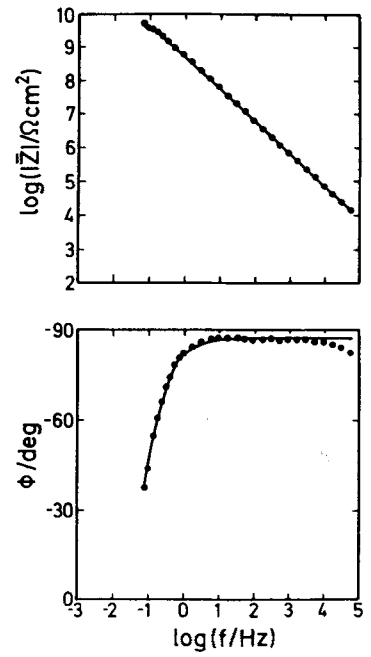

FIGURE 5. *Fit of the experimental data of curve (a) in Figure 2 with the modified Model A according to Equation (2). Fit parameters: R_L = 6.0 × 10^9 Ω·cm², C_L = 2.8 × 10^{-10} F·cm^{-2}, α = 0.97.*

C_L, but may affect the absolute value of $R_{\Omega,por}$ for $(1 - \theta) \ll 1$. Therefore, delamination effects can be better correlated to the width of the plateau at medium frequencies originated by $R_{\Omega,por}/(1 - \theta)$. This plateau width is determined by the effective capacitances θC_L and $(1 - \theta)C_{dl}$ as can be seen in Figure 6.

As is shown in Table 1b, the organic coating layer capacitance, C_L, remains nearly constant. The corresponding low variation of the dielectric constant ε indicates that the organic coating material changes only very slightly. Water uptake of the organic coating can be neglected. This holds even for much longer times of continuous exposure (up to half a year) of coatings of this type without local defects. For the samples under test, the pore resistances, $R_{\Omega,por}$, tend to decrease within the first 24-h exposure time, but can increase afterwards. This effect can be explained by a partial plugging of the pore channels with corrosion products and an increasing difference between θ_1 and θ_2 with increasing exposure time. The polarization resistance, R_p, increases significantly on bare steel and remains nearly constant on phosphated steel with exposure time. The increase of R_p on bare steel may be connected to the formation of porous corrosion product layers acting as an interphase inhibitor on the corroding metal surface. This is obviously not the case on phosphated steel. The active surface area $(1 - \theta)\mathbf{A}$ increases with the exposure time in good agreement with an observed delamination of the coating from the metallic substrate. However, visual verification of delamination (Figure 9) requires considerably longer exposure time than the 48 hours for the Table 1 data.

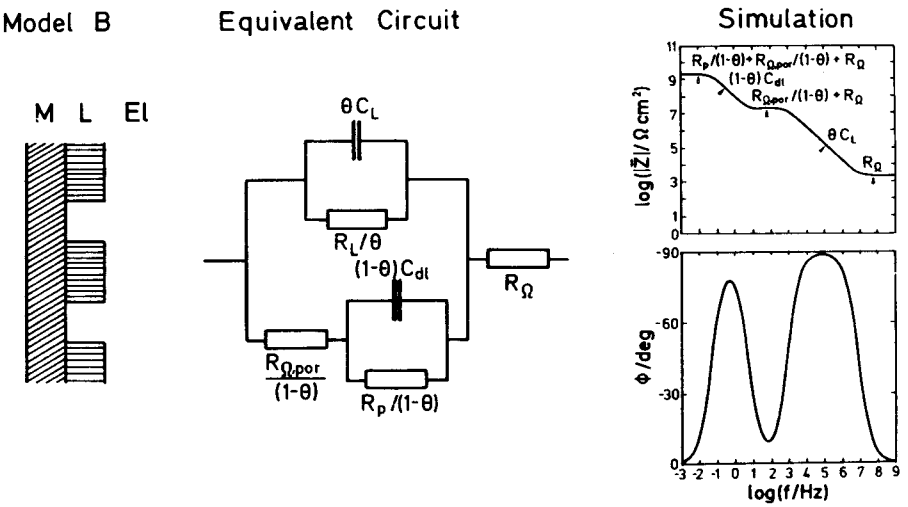

FIGURE 6. *Inhomogeneous 3-D surface layer Model B according to Equations (3) and (6). Simulation parameters:* $R_\Omega = 20\Omega{\cdot}cm^2$, $R_L = 10^{10}\ \Omega{\cdot}cm^2$, $C_L = 10^{-9} F{\cdot}cm^{-2}$, $\alpha = 1$, $R_{\Omega,por} = 10^3\ \Omega{\cdot}cm^2$, $R_P = 10^5\ \Omega{\cdot}cm^2$, $C_{dl} = 30 \times 10^{-6}\ F{\cdot}cm^{-2}$, $\theta = 0.995$.

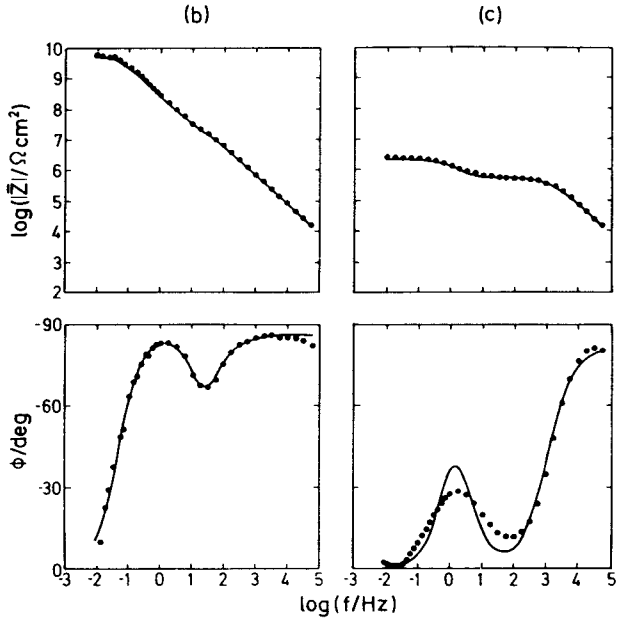

FIGURE 7. *Fit of the experimental data of curves (b) and (c) in Figure 2 with Model B according to Equations (2), (3), and (6). Fit parameters:*
Curve (b): $\theta C_L = 8.2.10^{-10}\ F{\cdot}cm^{-2}$, $\alpha = 0.96$, $R_{\Omega,por}/(1-\theta) = 3.5 \times 10^7\ \Omega{\cdot}cm^2$, $R_p/(1-\theta) = 5.6 \times 10^9\ \Omega{\cdot}cm^2$, $(1-\theta)C_{dl} = 2.7 \times 10^{-10}\ F{\cdot}cm^{-2}$.
Curve (c): $\theta C_L = 6.6 \times 10^{-9}\ F{\cdot}cm^{-2}$, $\alpha = 0.91$, $R_{\Omega,por}/(1-\theta) = 5.8 \times 10^5\ \Omega{\cdot}cm^2$, $R_p/(1-\theta) = 1.9 \times 10^6\ \Omega{\cdot}cm^2$ $(1-\theta(C_{dl} = 1.1 \times 10^{-7}\ F{\cdot}cm^{-2}$.

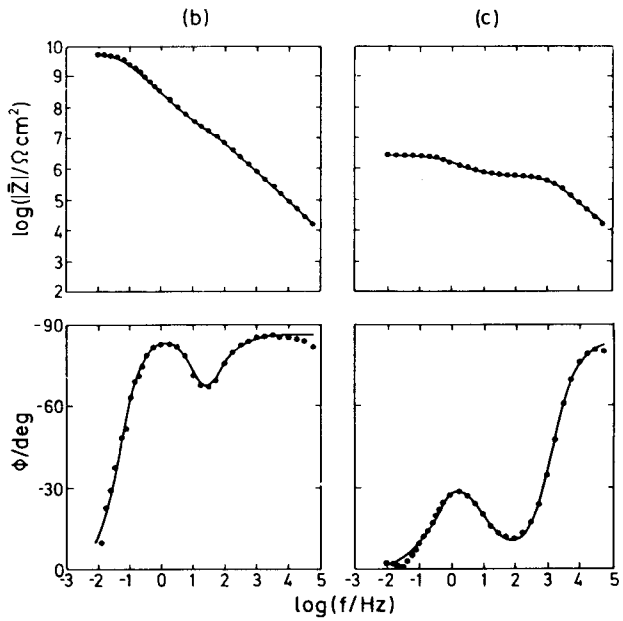

FIGURE 8. *Fit of the experimental data of curves (b) and (c) in Figure 2 with the modified Model B according to Equations (2), (3), and (7). Fit parameters:*
Curve (b): $\theta C_L = 2.9 \times 10^{-10}\ F{\cdot}cm^{-2}$, $\alpha = 0.96$, $R_{\Omega,por}/(1-\theta) = 3.3 \times 10^7\ \Omega{\cdot}cm^2$, $R_p/(1-\theta) = 5.6 \times 10^9\ \Omega{\cdot}cm^2$, $(1-\theta)C_{dl} = 2.8 \times 10^{-10}\ F{\cdot}cm^{-2}$, $\alpha' = 0.99$.
Curve (c): $\theta C_L = 3.9 \times 10^{-10}\ F{\cdot}cm^{-2}$, $\alpha = 0.94$, $R_{\Omega,\ por}/(1-\theta) = 5.0 \times 10^5\ \Omega{\cdot}cm^2$, $R_p/(1-\theta) = 2.3 \times 10^6\ \Omega{\cdot}cm^2$, $(1-\theta)C_{dl} = 1.8 \times 10^{-7}\ F{\cdot}cm^{-2}$, $\alpha = 0.70$.

The physical meaning of the exponent α' in Equation (7) is usually interpreted by either transmission line effects[3,4,7–14] or surface and/or film inhomogeneities.[1,4,20–22,25–30] Previously it has been shown[20–22] that corrosion processes in the presence of porous 3-D layers consisting of corrosion products or oxides can also be analyzed using a 3-D surface inhomogeneity model with the approximations

$$Z_{Sr,a}(s)/(1-\theta) \approx R_{Me} \qquad (8)$$

and

$$Z_{Sr,c}(s)/(1-\theta) \approx Z_{T,eff} \qquad (9)$$

where R_{Me} denotes a mean resistance for the mainly charge-transfer controlled metal dissolution process, which depends on the electrode potential, and $Z_{T,eff}$ is an effective transport impedance for a mainly mass-transport controlled cathodic corrosion reaction, both processes occurring at the bottom of the pores:

TABLE 1a
Optimum Fit Parameters of Impedance Data[A] for Imperfect Organic Coatings (A) and (B) on Bare and Phosphated Mild Steel

System	t (h)	θC_L ($F \cdot cm^{-2}$)	$R_{\Omega,por}/(1-\theta)$ ($\Omega \cdot cm^2$)	$R_p/(1-\theta)$ ($\Omega \cdot cm^2$)	$(1-\theta)C_{dl}$ ($F \cdot cm^{-2}$)	α	α'
bare steel/ coating (A)	0.25	3.24×10^{-10}	1.05×10^{9}	2.17×10^{9}	1.74×10^{-11}	0.959	1.000
	24	5.93×10^{-10}	4.40×10^{5}	7.15×10^{7}	7.55×10^{-9}	0.908	0.817
	48	3.24×10^{-10}	8.56×10^{6}	1.07×10^{7}	5.74×10^{-7}	0.960	0.758
bare steel/ coating (B)	0.25	6.74×10^{-10}	1.30×10^{6}	5.31×10^{7}	4.60×10^{-9}	0.900	0.787
	24	2.88×10^{-10}	6.17×10^{3}	1.77×10^{7}	1.61×10^{-7}	0.964	0.698
	48	3.93×10^{-10}	9.72×10^{4}	1.48×10^{7}	5.08×10^{-7}	0.940	0.745
phosphated steel/ coating (A)	0.25	2.93×10^{-10}	2.18×10^{8}	5.61×10^{9}	6.04×10^{-11}	0.962	1.000
	1	2.86×10^{-10}	3.28×10^{7}	5.59×10^{9}	2.79×10^{-10}	0.962	0.988
	48	3.93×10^{-10}	5.04×10^{5}	2.32×10^{6}	1.82×10^{-7}	0.939	0.702
phosphated steel/	0.25	2.72×10^{-10}	6.20×10^{7}	5.89×10^{9}	5.32×10^{-12}	0.974	0.958
	24	2.84×10^{-10}	4.61×10^{7}	1.58×10^{7}	1.49×10^{-9}	0.970	1.000

[A]Depending on the exposure time, t, using the modified Model B according to Equations (2), (3), and (7).

TABLE 1b
Calculated Specific Parameters[A] for Imperfect Organic Coatings (A) and (B) on Bare and Phosphated Mild Steel

System	t (h)	C_L ($F \cdot cm^{-2}$)	$R_{\Omega,por}$ ($\Omega \cdot cm^2$)	R_p ($\Omega \cdot cm^2$)	θ	Active Surface Area $(1-\theta)A$ (cm^2)
bare steel/ coating (A)	0.25	3.24×10^{-10}	7.31×10^{2}	1.51×10^{3}	0.99999930	1.39×10^{-5}
	24	5.93×10^{-10}	1.33×10^{2}	2.16×10^{4}	0.99969800	6.04×10^{-3}
	48	3.32×10^{-10}	1.97×10^{5}	2.46×10^{5}	0.97704000	4.59×10^{-1}
bare steel/ coating (B)	0.25	6.74×10^{-10}	2.39×10^{2}	9.77×10^{3}	0.99981600	3.68×10^{-3}
	24	2.90×10^{-10}	3.97×10^{1}	1.14×10^{5}	0.99356000	1.29×10^{-1}
	48	4.01×10^{-10}	1.98×10^{3}	3.01×10^{5}	0.97968000	4.06×10^{-1}
phosphated steel/ coating (A)	0.25	2.93×10^{-10}	5.27×10^{2}	1.36×10^{4}	0.99999758	4.83×10^{-5}
	1	2.86×10^{-10}	3.66×10^{2}	6.24×10^{4}	0.99998884	2.23×10^{-4}
	48	3.96×10^{-10}	3.67×10^{3}	1.69×10^{4}	0.99272000	1.46×10^{-1}
phosphated steel/	0.25	2.72×10^{-10}	1.32×10^{1}	$1..25 \times 10^{3}$	0.99999978	4.26×10^{-6}
	24	2.84×10^{-10}	2.75×10^{3}	9.42×10^{2}	0.99994040	1.19×10^{-3}

[A]Depending on the exposure time, t, using the modified Model B according to Equations (2), (3), and (7).

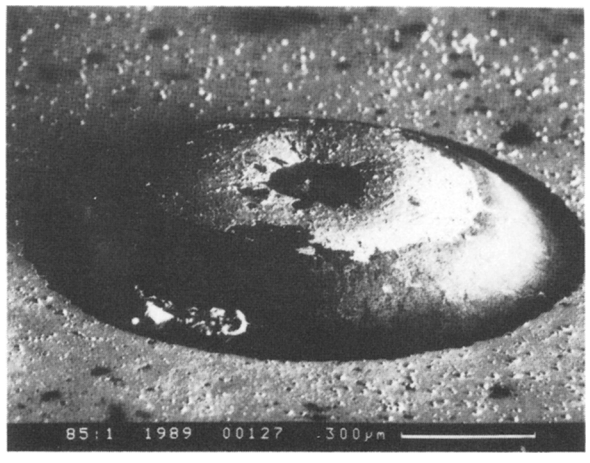

FIGURE 9. *SEM study of a local defect in organic coating (A) on phosphated steel after an exposure time of $t = 10^3$ h.*

$$Z_{T,eff}(s) = R_{T,eff} \frac{\text{th } l_{eff}[(s + W)/D]^{1/2}}{l_{eff}[(s + W)/D]^{1/2}} \quad (10)$$

where $R_{T,eff}$ denotes an effective transport resistance, l_{eff} is an effective diffusion length, W represents a rate constant for lateral transport effects, and D is the diffusion coefficient of the electroactive species.

An application of this Model C with 8 adjustable fit parameters (θC_L, α, $R_{\Omega,por}/(1-\theta)$, R_{Me}, $R_{T,eff}$, l_{eff}, W, and $(1-\theta)C_{dl}$) to the experimental data typically represented by curves (b) and (c) in Figure 2 does not give significantly better fits. This means that the system under test is reasonably characterized by the 6 adjustable fit parameters (θC_L, $R_{\Omega,por}/(1-\theta)$, $R_p/(1-\theta)$, $(1-\theta)C_{dl}$, α, and α') of the semi-empirical Model B described by Equations (2), (3), and (7). However, the transfer function is actually affected by a restricted number of only 3 parameters within a particular frequency range as shown schematically in Figure 6. Obviously, a separation of the components of $Z_{SR}(s)$ becomes difficult for relatively high values of $R_{\Omega,por}/(1-\theta)$.[14]

Summarizing the results of Table 1, the organic coating (B) on phosphated steel shows a better bonding to the substrate than coating (A) indicated by the values of the active surface area. On bare steel, both organic coatings show much higher delamination effects with increasing exposure time.

The results in Table 1 depend to a certain extent on small defects of the coating (random in number and size) existing in the studied surface area of the sample. In order to eliminate such undefined effects, organic coatings (A) and (B) on mild steel were investigated by EIS depending on the exposure time after drilling artificial pores of 0.01-cm diameter. The results after exposure at the open-circuit potential and after cathodic disbonding are summarized in Tables 2 and 3, respectively.

Optimum fits of the experimental data in Tables 2a and 3a and the calculated specific parameters in Tables 2b and 3b were obtained using either the modified Model B according to Equations (2), (3), and (7) or Model C according to Equations (2) through (5) with the approximations in Equations (8) through (10) as demon-

TABLE 2a
Optimum Fit Parameters of Impedance Data[A] for Organic Coatings (A) and (B) with Drilled Artificial Pores on Bare Mild Steel

System	t (h)	θC_L ($F \cdot cm^{-2}$)	$R_{\Omega,por}/(1-\theta)$ ($\Omega \cdot cm^2$)	$R_p/(1-\theta)$ ($\Omega \cdot cm^2$)	$(1-\theta)C_{dl}$ ($F \cdot cm^{-2}$)	α	α'
bare steel/ coating (A)	0.25	2.95×10^{-10}	5.94×10^{4}	6.54×10^{7}	2.80×10^{-8}	0.956	0.572
	24	2.93×10^{-10}	7.67×10^{4}	2.00×10^{7}	5.52×10^{-7}	0.966	0.640
	264	3.54×10^{-10}	5.74×10^{6}	5.46×10^{6}	1.81×10^{-7}	0.954	0.397
bare steel/ coating (B)	0.25	2.63×10^{-10}	7.10×10^{4}	7.27×10^{7}	2.77×10^{-9}	1.000	0.738
	24	2.38×10^{-10}	4.87×10^{5}	1.84×10^{7}	1.41×10^{-6}	0.996	0.816
	264	3.13×10^{-10}	1.33×10^{7}	8.45×10^{6}	1.04×10^{-7}	0.970	0.607

[A]Depending on the exposure time, t, using the modified Model B according to Equations (2), (3), and (7).

TABLE 2b
Calculated Specific Parameters[A] for Organic Coatings (A) and (B) with Drilled Artificial Pores on Bare Mild Steel

System	t (h)	C_L ($F \cdot cm^{-2}$)	$R_{\Omega,por}$ ($\Omega \cdot cm^2$)	R_p ($\Omega \cdot cm^2$)	θ	Active Surface Area $(1-\theta)A$ [cm^2]
bare steel/ coating (A)	0.25	2.95×10^{-10}	6.65×10^{1}	7.32×10^{4}	0.99888000	2.24×10^{-2}
	24	3.00×10^{-10}	1.69×10^{3}	4.42×10^{5}	0.97792000	4.42×10^{-1}
	264	3.57×10^{-10}	4.16×10^{4}	3.95×10^{4}	0.99276000	1.45×10^{-1}
bare steel/ coating (B)	0.25	2.63×10^{-10}	7.87×10^{0}	8.06×10^{3}	0.99988920	2.22×10^{-3}
	24	2.52×10^{-10}	2.75×10^{4}	1.04×10^{6}	0.94360000	1.13×10^{0}
	264	3.14×10^{-10}	5.53×10^{4}	3.52×10^{4}	0.99584000	8.32×10^{-2}

[A]Depending on the exposure time, t, using the modified Model B according to Equations (2), (3), and (7).

TABLE 3a
Optimum Fit Parameters of Impedance Data[A] for Cathodically Disbonded Organic Coatings (A) and (B) with Drilled Artificial Pores on Bare Mild Steel

System	t (h)	θC_L ($F \cdot cm^{-2}$)	$R_{\Omega,por}/(1-\theta)$ ($\Omega \cdot cm^2$)	$R_p/(1-\theta)$ ($\Omega \cdot cm^2$)	$(1-\theta)C_{dl}$ ($F \cdot cm^{-2}$)	α	α'
bare steel/ coating (A)	0.25	2.78×10^{-10}	3.75×10^{4}	3.95×10^{7}	9.88×10^{-9}	1.000	0.820
	2	2.84×10^{-10}	6.01×10^{4}	3.88×10^{7}	4.77×10^{-8}	1.000	0.653
	96	3.01×10^{-10}	4.53×10^{4}	3.58×10^{7}	7.08×10^{-8}	1.000	0.705
bare steel/ coating (B)	4	2.43×10^{-10}	6.01×10^{4}	2.62×10^{7}	1.15×10^{-8}	1.000	0.733
	58	2.42×10^{-10}	7.20×10^{4}	1.35×10^{6}	5.91×10^{-7}	1.000	0.810

[A]Depending on the exposure time, t, using the modified Model B according to Equations (2), (3), and (7).

TABLE 3b
Calculated Specific Parameters[A] for Cathodically Disbonded Organic Coatings (A) and (B) with Drilled Artificial Pores on Bare Mild Steel

System	t (h)	C_L ($F \cdot cm^{-2}$)	$R_{\Omega,por}$ ($\Omega \cdot cm^2$)	R_p ($\Omega \cdot cm^2$)	θ	Active Surface Area $(1-\theta)A$ (cm^2)
bare steel/ coating (A)	0.25	2.78×10^{-10}	1.48×10^{1}	1.56×10^{4}	0.99960480	7.90×10^{-3}
	2	2.85×10^{-10}	1.15×10^{2}	7.40×10^{4}	0.99809200	3.82×10^{-2}
	96	3.02×10^{-10}	1.28×10^{2}	1.01×10^{5}	0.99716800	5.66×10^{-2} (9.00×10^{-2})
bare steel/ coating (B)	4	2.43×10^{-10}	2.76×10^{1}	1.21×10^{4}	0.99954000	9.20×10^{-3}
	58	2.48×10^{-10}	1.70×10^{3}	3.19×10^{4}	0.97636000	4.73×10^{-1} (4.40×10^{-1})

[A]Depending on the exposure time, t, using the modified Model B according to Equations (2), (3), and (7). The active surface areas given in parentheses correspond to adhesive pulling-off at the end of the tests.

strated in Figure 10. Obviously, the accuracy of the experimental data is not sufficient enough to distinguish between Models B and C.

The results in Table 2b show a strong increase of $R_{\Omega,por}$ with extended exposure time which must be due to the plugging of the drilled pores with corrosion products since the effective values $R_{\Omega,por}/(1 - \theta)$ even increase strongly. In this case, the corrosion process at the metal/coating interface can no longer be analyzed quantitatively. In order to eliminate these complications, cathodic polarization was applied to suppress the anodic metal dissolution process and to enhance the delamination effect.

The prerequisite to the assumption $C_{dl} \approx 25 \times 10^{-6}$ F·cm^{-2}, namely a quasi-homogeneous surface, is best met under this condition. The data in Table 3b show a continuous increase of the delaminated surface area with increasing exposure time. This is also evident from the increasing width of the plateau caused by $R_{\Omega,por}/(1 - \theta)$. The result presented in Table 3 show clear differences in the delamination behavior of the coatings (A) and (B), which is in very good agreement with conventional non-electrochemical exposure tests such as salt spray and climate-changing testing.[31]

The active surface areas obtained by EIS and given in Table 3b are in a good agreement with optical measurements of the delaminated surface area after adhesive pulling-off. These values are given in Table 3b in brackets. Calculating C_{dl} from these data yields $C_{dl} \approx 22 \times 10^{-6}$ to 25×10^{-6} F·cm^{-2}, which is in agreement with the assumptions made above.

A Warburg-like behavior of organic coatings on phosphated steel at relatively low frequencies has been reported by Mansfeld et al.[9,14] This effect was attributed to an inhomogeneous current distribution caused by the formation of phosphate crystals leading to transmission line effects. In the present study, the relatively low values of α' in Tables 2b and 3b may also be caused by an inhomogeneous current distribution due to a partial blocking of the metal surface by corrosion products and complicated mass transport processes within the pores.

CONCLUSIONS

▶ EIS measurements of organic coatings on steel exposed to neutral aqueous solutions provide a powerful tool to characterize their corrosion protection value. In this paper, the transfer function analysis is carried out to describe quantitatively perfect and imperfect coatings using the quasi-homogeneous 3-D surface Model A and the inhomogenous 3-D surface Models B and C. It is demonstrated that Model B is a simplification of Model C and Model A represents the limiting case of Model C for $R_{\Omega,por} \rightarrow \infty$, i.e., the perfect coating. The imperfect coatings show 3-D inhomogeneity effects which can be taken into account either by an empirical exponent α in the Model B or by lateral transport contributions of the corrosion reaction in Model C. The corrosion process at the metal/coating interface is well described at relatively low frequencies by the polarization resistance, R_p, in Model B, the anodic charge transfer resistance, R_{Me}, and the cathodic transport impedance, $Z_{T,eff}$, in Model C as well as the double-layer capacitance, C_{dl}. EIS has a high sensitivity to detect local defects within the organic coating characterized by $R_{\Omega,por}$. It is proposed that delamination effects can be estimated from the width of the plateau caused by $R_{\Omega,por}$ in the medium frequency range. The capacitance of the organic coating, C_L, can be determined from the high-frequency part of impedance spectra even of damaged films in the presence of sufficiently high values of $R_{\Omega,por}$. The film resistance, R_L, can only be approximated from low-frequency impedance data of undamaged organic coatings.

▶ The characterization of the corrosion protection by imperfect organic coatings can become difficult for long-time exposure at the corrosion potential if insoluble corrosion products cover the anodic area at the metal/electrolyte interface and plug the pores. Therefore, delamination effects can be better characterized using cathodic polarization conditions avoiding these complications. Cathodic polarization also accelerates the disbonding of the organic coating. This technique generally agrees with different testing standards such as ASTM[(6)] G 8 or G 42.

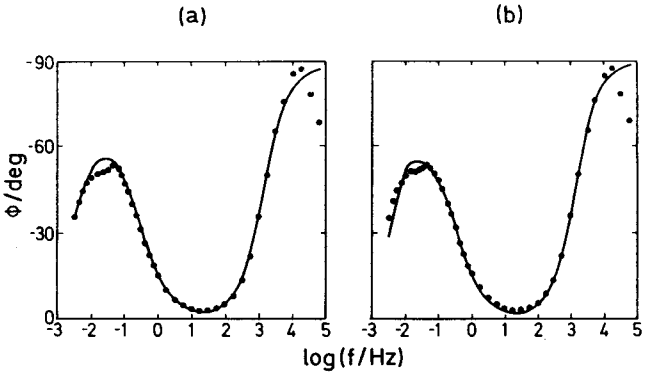

FIGURE 10. *Fit of experimental phase angle data (x) obtained on organic coating (B) with one drilled artificial pore of 0.01-cm diameter on bare mild steel after an exposure time of 24 h at the open-circuit potential:*
(a) Fit corresponding to the modified Model B according to Equations (2), (3), and (7). Fit parameters: $\theta C_L = 2.4 \times 10^{-10}$ F·cm^{-2}, $\alpha = 0.99$ $R_{\Omega,por}/(1 - \theta) = 4.9 \times 10^5$ Ω·cm^2, $R_p/(1 - \theta) = 1.8 \times 10^7$ Ω·cm^2, $(1 - \theta)C_{dl} = 1.4 \times 10^{-6}$ F·cm^{-2}, $\alpha = 0.82$.
(b) Fit corresponding to Model C according to Equations (2) through (5) with the approximations in Equations (8) through (10). Fit parameters: $\theta C_L = 2.4 \times 10^{-10}$ F·cm^{-2}, $\alpha \approx 1$, $R_{\Omega,por}/(1 - \theta) = 4.9 \times 10^5$ Ω·cm^2, $R_{Me} \approx 10^{15}$ Ω·cm^2, $R_{T,eff} = 1.3 \times 10^7$, $l_{eff} = 0.021$ cm, $W \approx 0$ s^{-1}, $(1 - \theta)C_{dl} = 9.3 \times 10^{-7}$ F·cm^{-2}.

ACKNOWLEDGMENT

The authors thankfully acknowledge the cooperation between BASF Aktiengesellschaft Ludwigshafen and the University of Karlsruhe.

This work is dedicated to Dr. Günter Bogenstätter, Director of Technical Development, BASF Aktiengesellschaft, Ludwigshafen, FRG, on the occasion of his 60th birthday.

REFERENCES

1. K. Jüttner, W.J. Lorenz, W. Paatsch, M.W. Kendig, and F. Mansfeld, Werkstoffe und Korrosion 36(1985): p. 120.
2. H. Leidheiser, "Coatings," in Corrosion Mechanisms, ed. F. Mansfeld, (New York, NY: Marcel Dekker, 1987), p. 165.
3. J.R. Macdonald, Impedance Spectroscopy (New York, NY: John Wiley & Sons,1987), p. 306.
4. F. Mansfeld and W.J. Lorenz, "Electrochemical Impedance Spectroscopy - Application in Corrosion Science and Technology," in Techniques for Characterization of Electrodes and Electrochemical Processes, ed. R. Varma and J.R. Selman, Electrochem Soc. Monograph Series (New York, NY: John Wiley and Sons, in print).
5. L. Beaunier, I. Epelboin, J.C. Lestrade and H. Takenouti, Surf. Technol. 4(1976): p. 137.
6. S. Haruyama, M. Asari, and T. Tsuru, "Impedance Characteristics during Degradation of Coated Steel," in Proceedings of the Symposium on Corrosion Protection by Organic Coatings, Vol. 87-2 (Pennington, NJ: The Electrochemical Society, 1987), p. 197.
7. F. Mansfeld, M.W. Kendig, and S. Tsai, Corrosion 38(1982): p. 478.
8. M.W. Kendig, F. Mansfeld, and S. Tsai, Corrosion Sci. 23(1983): p. 317.
9. F. Mansfeld and M.W. Kendig, ASTM STP 866(1985): p. 122.
10. F. Mansfeld and M.W. Kendig, Corrosion 41(1985): p. 490.
11. F. Mansfeld and M.W. Kendig, Materials Science Forum 8,(1986): p. 337.
12. F. Mansfeld, S.L. Jeanjaquet, and M.W. Kendig, Corrosion Sci. 26(1986): p. 735.

(6) American Society for Testing and Materials (ASTM), Philadelphia, PA.

13. F. Mansfeld, Corrosion 44(1988): p. 856.
14. F. Mansfeld and C.H. Tsai, submitted to Corrosion.
15. W. Siedlarek, W. Mader, and W. Fischer, Farbe und Lacke 90(1984): p. 824.
16. M. Ebert, Diplomarbeit Universitat Karlsruhe 1986.
17. G.H. Wagner, Pitture e vernici 7(1984): p. 105.
18. M.W. Kendig, A.T. Allen, F. Mansfeld J. Electrochem. Soc. 131(1984): p. 935.
19. F. Mansfeld, M.W. Kendig, and W.J. Lorenz, J. Electrochem. Soc. 132(1985): p. 290.
20. K. Jüttner, K. Manandhar, U. Seifer-Kraus, W.J. Lorenz, and E. Schmidt, Werkstoffe und Korrosion 37(1986): p. 377.
21. K. Jüttner, W.J. Lorenz, M.W. Kendig, and F. Mansfeld, J. Electrochem Soc. 135(1988): p. 335.
22. M. Mitzlaff, H.N. Hoffmann, K. Jüttner, and W.J. Lorenz, Ber. Bunsenges. Phys. Chem. 92(1988): p. 1234.
23. W.J. Lorenz and H. Fischer, Electrochim. Acta 11(1966): p. 1597.
24. W.J. Lorenz, K. Sarropoulos, and H. Fischer, Electrochim. Acta 14(1969): p. 179.
25. J. Hitzig, K. Jüttner, W.J. Lorenz, and W. Paatsch, J. Electrochem. Soc. 133(1986): p.887.
26. W. Paatsch, W.J. Lorenz, and K. Jüttner, Metalloberflache 41(1987): p. 282.
27. K. Jüttner and W.J. Lorenz, "Dynamic System Analysis in Corrosion Research and Testing," in Proceedings of the 10th International Congress on Metallic Corrosion, vol. 1 (New Delhi, India: Oxford & IBH Publishing, 1987), p. 457.
28. K. Jüttner, W.J. Lorenz, and W. Paatsch, Corrosion Sci. 29(1989): p. 279.
29. K. Jüttner and W.J. Lorenz, Materials Science Forum 44 and 45 (1989): p. 191.
30. K. Jüttner and W.J. Lorenz, "Surface Inhomogeneity Characterized by EIS," in Proceedings of the Symposium on Transient Techniques in Corrosion Science and Engineering, vol. 89–1 (Pennington, NJ: The Electrochemical Society Inc., 1989), p. 68.
31. J. Titz and G.H. Wagner, BASF Internal Research Report (Ludwigshafen, FRG: BASF, 1989).

Some Advantages and Pitfalls of Electrochemical Impedance Spectroscopy ☆

D.D. Macdonald

ABSTRACT

The use of electrochemical impedance spectroscopy (EIS) in corrosion research is briefly reviewed with particular emphasis on the advantages offered by this technique over other electrochemical methods. These advantages include the fact that it is a steady-state technique, that it employs small signal analysis, and that is capable of probing relaxations over a very wide frequency range (<1 mHz to >1 MHz) using readily available istrumentation. EIS also has the enormous advantage over classical transient techniques in that the validity of the data is readily checked using the Kramers–Kronig transforms. The principal pitfall of the method is the tendency of many workers to analyze their data in terms of simple equivalent electrical circuits, and hence to ignore the great power of EIS for deriving mechanistic and kinetic information for processes that occur at a corroding interface.

KEY WORDS: corrosion rate, electrochemical impedance spectroscopy, reaction mechanisms.

INTRODUCTION

Electrochemical impedance spectroscopy (EIS) is now well established[1-5] as a powerful technique for investigating electrochemical and corrosion systems. The power of EIS lies in the fact that it is essentially a steady-state technique that is capable of accessing relaxation phenomena whose relaxation times vary over many orders of magnitude. The steady-state character permits the use of signal averaging within a single experiment to gain the desired level of precision, and the wide frequency bandwidth (10^6 to 10^{-4} Hz) that is now available using transfer function analyzers permits a wide range of interfacial processes to be investigated. These features generally surpass the equivalent performance characteristics for time domain experimental techniques,[4] so that EIS has rapidly developed as one of the principal methods for investigating interfacial reaction mechanisms.

In this paper, the foundations of EIS are briefly reviewed with particular emphasis on corrosion science and engineering. Because impedance spectroscopy is a relatively new technique, at least in its application in corrosion science and electrochemistry, its theoretical basis has not been extensively treated in standard texts. Accordingly, we begin this review by discussing, in very general terms, transfer-function analysis before progressing to the much more specific task of illustrating the advantages and pitfalls of EIS as it is employed in the study of corrosion processes.

Unfortunately, there is no "easy" way of developing the skills and expertize necessary to properly interpret impedance data. Accordingly, it is essential that the reader follow the mathematical developments presented in this paper, as well as develop an appreciation for the electrochemistry involved in the various analytical techniques. Because this paper is intended to be tutorial in nature and to illustrate some of the advantages and pitfalls of EIS, the essential mathematical arguments are developed in detail and in some length, rather than simply stating the problem and presenting the solution. While this renders the discussion somewhat verbose, it does allow the reader who is not familiar with EIS to grasp the mechanics of analyzing impedance data. Where appropriate, the analytical methods are illustrated by reference to experimental studies that have been reported in the literature.

FUNDAMENTALS

The response of any linear system to a perturbation of arbitrary form may be described by a transfer function

$$H(s) = \bar{V}(s)/\bar{I}(s) \qquad (1)$$

where s is the Laplace frequency, and $\bar{V}(s)$ and $\bar{I}(s)$ are the Laplace transforms of the time-dependent voltage and current, respectively.[6] In terms of the steady-state sinusoidal frequency domain, the transfer function becomes

☆ Submitted for publication May 1989; in revised form, October 1989. Presented as paper no. 30 at CORROSION/89 in New Orleans, Louisiana, April 1989.

* SRI International, 333 Ravenswood Ave., Menlo Park, CA 94025.

0010-9312/90/000071/$3.00/0

